Chapter 2

Nonlinear Finite Element Formulation for The Postbuckling Analysis of Stiffened Composite Panels with Imperfections

Those concepts behind the Finite Element method which are useful in applying the basic theory to the postbuckling analysis of stiffened composite panels will be briefly outlined in this chapter. However, no attempt will be made to present in detail the Finite Element method, or the fundamental equations of the nonlinear theory of elasticity. This material can be found in [35].

First the large deflection problem is intrinsically different from the small deflection problem. This is so, not because large deflections necessarily occur in a literal sense, but rather because stresses exist which, in the presence of certain displacements, exert a significant influence on structural deformations. The beam-column problem illustrates this typical, large deflection behavior. Existence of axial loading in the presence of bending displacements does affect the stiffness of the member. In fact, if the loading is compressive and approaches the critical value, the bending stiffness tends toward zero. Consequently, the need for an “initial stress stiffness matrix” becomes evident.

Two sources of nonlinearity exist for the large deflection problem. The first is connected with the strain-displacement equations. Even if strains remain small in the conventional sense, rotation of the element adds nonlinear terms to the strain-displacement equation. As will be seen in the derivation of the plate element, if these nonlinear, rotational terms are omitted, the derivation becomes incapable of yielding the nonlinear stiffness matrix.

The second source of nonlinearity exists with respect to the equilibrium equations. It is necessary to keep the deformed geometry in mind when writing the equilibrium equations. This in turn, causes these equations to become nonlinear. In the Finite Element method, this is taken into account at the start of each step. In this manner a close approximation to the actual behavior can be maintained.

It is therefore seen that the Finite Element method accounts for both sources of nonlinearity in the large deflection problem. Entering into the derivation of the stiffness matrices through the strain-displacement equations is sufficient for stability analyses. By using the stiffness matrices so derived, in conjunction with the incremental step procedure, corrections in the equilibrium equations due to structural deformation can be taken into account. This makes it possible to carry out a detailed analysis of the large deflection problem.

In this chapter, we start by introducing the variational equations of equilibrium along with the derived element equilibrium equations. Then the stiffness formulation for a 4-node, 6-degree-of freedom per node rectangular plate element is presented. A brief description of the integration technique employed is then given followed by a short introduction to the frontal solution technique used in this study. Finally, the nonlinear incremental solution procedure is described followed by example problems demonstrating the convergence of the results obtained by the developed element to the published exact and experimental solutions for composite panels under inplane and transverse loading.

2.1 Variational Equation of Equilibrium

The total potential energy Π of a deformed plate with initial deflection of the order of magnitude of the thickness and with additional bending deflection of the same order, is defined as

$$\Pi = U - W \tag{2.1}$$

where U is the potential energy of deformation and W is the potential energy of the external loading.

The state of equilibrium of a deformed plate can be characterized as that for which the first variation of the total potential energy of the system is equal to zero

$$\delta\Pi = \delta U - \delta W = 0 \tag{2.2}$$

or

$$\delta U = \delta W \tag{2.3}$$

The potential energy of the external load is

$$W = p_i \, q_i \tag{2.4}$$

in which the repeated indices imply summation, p_i is the external load, and q_i is the displacement. Thus, if the displacements are defined by a finite number of nodal parameters $\vec{a}$, the variation in the potential energy of the external load is

$$\delta W = \vec{f} \, d\vec{a} \tag{2.5}$$

where $\vec{f}$ is a vector of generalized external forces.

The variation in the potential energy of deformation for a plate element with large deflection can be written as

$$\delta U = (\int_V [\bar{B}]^T \vec{\sigma}\, dV)\, d\vec{a} \tag{2.6}$$

where $[\bar{B}]$ is defined from the strain definition as

$$d\vec{\varepsilon} = [\bar{B}]\, d\vec{a} \tag{2.7}$$

The bar suffix has been added as, if displacements are large, the strains depend nonlinearly on displacements, and the matrix $[\bar{B}]$ depends on $\vec{a}$. We shall see later that we can conveniently write

$$[\bar{B}] = [B_o] + [B_L(\vec{a})] \tag{2.8}$$

in which $[B_o]$ is the same matrix as in the linear infinitesimal strain analysis and only $[B_L]$ depends on the displacement. In general $[B_L]$ is found to be a linear function of the displacements.

Substituting from Equations (2.6) and (2.5) into Equation (2.2) we get the equilibrium equations written as

$$\vec{\Psi}(\vec{a}) = \int_V [\bar{B}]^T \vec{\sigma}\, dV - \vec{f} = 0 \tag{2.9}$$

where $\vec{\Psi}$ represents the sum of external and internal generalized forces.

Clearly, solution of Equation (2.9) will have to be approached iteratively. In order to use an incremental solution procedure, the relation between $d\bar{a}$ and $d\bar{\Psi}$ must be found. Thus, taking appropriate variation of Equation (2.9) with respect to $d\bar{a}$ we have

$$d\bar{\Psi} = \int_V d[\overline{B}]^T \, \bar{\sigma} \, dV + \int_V [\overline{B}]^T \, d\bar{\sigma} \, dV = [K_T] \, d\bar{a} \tag{2.10}$$

$[K_T]$ being the total tangential stiffness matrix. If strains are reasonably small, we can write the general elastic relation

$$\bar{\sigma} = [D] \bar{\varepsilon} \tag{2.11}$$

in which $[D]$ is the usual set of elastic constants. Thus using Equations (2.11) and (2.7) we have

$$d\bar{\sigma} = [D] d\bar{\varepsilon} = [D][\overline{B}] \, d\bar{a} \tag{2.12}$$

and if (2.8) is valid

$$d[\overline{B}] = d[B_L] \tag{2.13}$$

Therefore

$$d\bar{\Psi} = \int_V d[B_L]^T \, \bar{\sigma} \, dV + [\overline{K}] \, d\bar{a} \tag{2.14}$$

where

$$[\overline{K}] = \int_V [\overline{B}]^T \, [D][\overline{B}] \, dV = [K_o] + [K_L] \tag{2.15}$$

In this expression $[K_o]$ represents the usual, small displacement stiffness matrix, i.e.

$$[K_o]=\int_V [B_o]^T [D][B_o]\,dV \tag{2.16a}$$

The matrix $[K_L]$ is due to large displacements and is given by

$$[K_L]=\int_V ([B_o]^T [D][B_L]+[B_L]^T [D][B_L]+[B_L]^T [D][B_o])\,dV \tag{2.16b}$$

$[K_L]$ is alternatively known as the *initial displacement matrix* or *large displacement matrix*, and contains only terms that are linear and quadratic in $\bar{a}$.

The first term of Equation (2.14) can be written as

$$\int_V d[B_L]^T \bar{\sigma}\,dV=[K_\sigma]\,d\bar{a} \tag{2.17}$$

where $[K_\sigma]$ is a symmetric matrix dependent on the stress level. This matrix is known as initial stress matrix or geometric matrix. Thus,

$$d\bar{\Psi}=([K_o]+[K_\sigma]+[K_L])\,d\bar{a}=[K_T]\,d\bar{a} \tag{2.18}$$

with $[K_T]$ being the total, tangential stiffness matrix.

In the next section, the tangential stiffness matrix for a rectangular plate element is derived in terms of the element shape functions and nodal displacements.

2.2 Stiffness Formulation for a Rectangular Plate Element

A typical rectangular laminated plate has dimensions *a* and *b* and thickness *t*. The laminate is composed of a number of perfectly bounded orthotropic layers (laminae) with different orientation angles. In a symmetric laminate, these laminae orientations are placed symmetrically with respect to the mid-plane. A coordinate system is adopted such that the *x*-*y* plane coincides with the mid-plane of the plate and the *z*-axis is perpendicular to the plane.

The nonlinear stiffness formulations for large deflection analysis of plates with initial imperfections are formulated for this typical rectangular plate finite element. The element is shown in Figure (2.1) with six degrees of freedom at each nodal point. These are : two inplane displacements *u* and *v* in the *x* and *y* directions, respectively; one transverse deflection *w*; two rotations $w_{,x}$ and $w_{,y}$ about the *y* and *x* axes, respectively, and a generalized twist $w_{,xy}$.

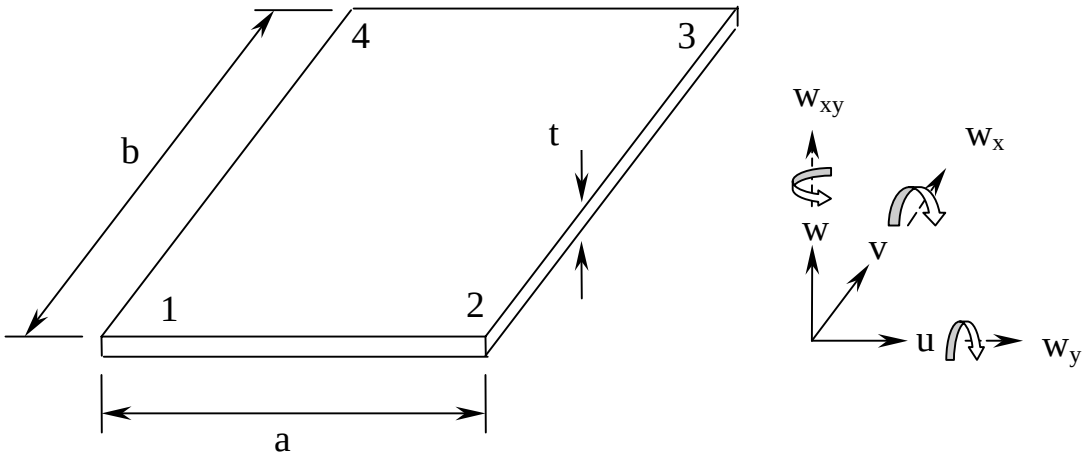

Figure (2.1) Element geometry and nodal degrees of freedom

The present element is based on Kirchoff plate theory [77] which neglects transverse shear deformation by assuming that straight lines normal to the mid-surface before deformation remain straight and normal to the mid-surface after deformation.

Knowing that the panels in this study have a width-to-thickness ratio of over 400, it is thus clear that we can neglect the transverse shear deformation effects without any significant loss in accuracy. The displacement model used in the formulation is thus given as [77]

$$u = u_o - z\frac{\partial w}{\partial x}$$

$$v = v_o - z\frac{\partial w}{\partial y} \qquad (2.19)$$

$$w = w_o$$

where u_o, v_o, w_o are the mid-plane displacements in the *x*, *y* and *z*-direction, respectively. Figure (2.2) shows the plate configuration before and after deformation. It is clear from Equations (2.19) that the displacement at any point inside the plate can be expressed in terms of five unknown quantities; $u_o, v_o, w_o, w_{,x}, w_{,y}$. However, the joint twist derivatives $w_{,xy}$ are adopted as extra degrees of freedom to assure inclusion of the strain due to simple twist.

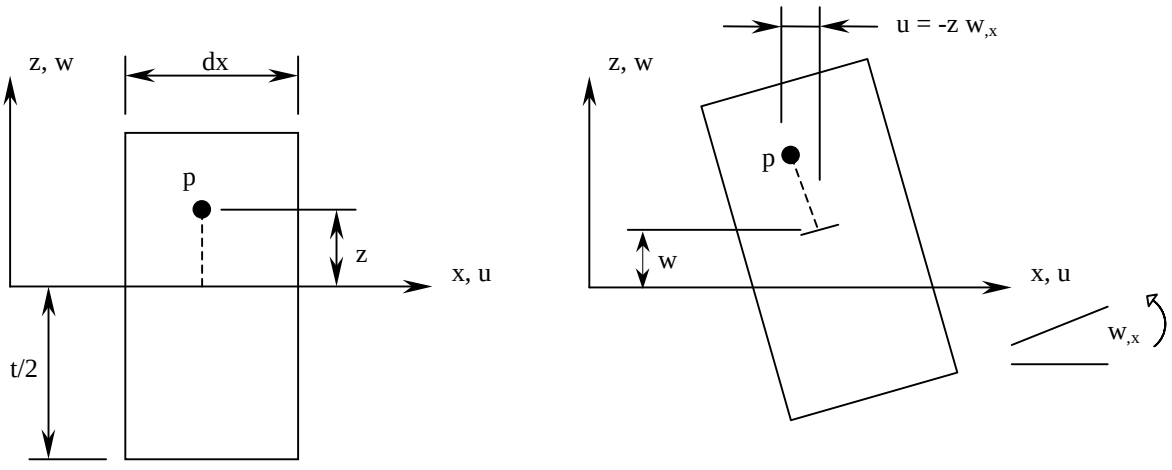

Figure (2.2) Kirchoff thin plate deformation model

2.2.1 Strain-Displacement Relations

The plate strains can be written in terms of the middle surface deflections as [78]

$$\varepsilon_x = \frac{\partial u}{\partial x} + \frac{1}{2}\frac{\partial w}{\partial x}\left(\frac{\partial w}{\partial x} + 2\frac{\partial w_o}{\partial x}\right) - z\frac{\partial^2 w}{\partial x^2}$$

$$\varepsilon_y = \frac{\partial v}{\partial y} + \frac{1}{2}\frac{\partial w}{\partial y}\left(\frac{\partial w}{\partial y} + 2\frac{\partial w_o}{\partial y}\right) - z\frac{\partial^2 w}{\partial y^2} \tag{2.20}$$

$$\gamma_{xy} = \frac{\partial u}{\partial y} + \frac{\partial v}{\partial x} + \frac{1}{2}\frac{\partial w}{\partial x}\left(\frac{\partial w}{\partial y} + 2\frac{\partial w_o}{\partial y}\right) + \frac{1}{2}\frac{\partial w}{\partial y}\left(\frac{\partial w}{\partial x} + 2\frac{\partial w_o}{\partial x}\right) + 2z\frac{\partial^2 w}{\partial x \partial y}$$

where w_o is the displacement function for the initial imperfection [78] and *u*, *v*, *w* stand for appropriate displacements of the middle surface.

Or in a more compact form

$$\{\varepsilon\} = \begin{Bmatrix} u_{,x} \\ v_{,y} \\ u_{,y} + v_{,x} \end{Bmatrix} + z\begin{Bmatrix} -w_{,xx} \\ -w_{,yy} \\ 2w_{,xy} \end{Bmatrix} + \frac{1}{2}\begin{Bmatrix} w_{,x}^2 \\ w_{,y}^2 \\ 2w_{,x}w_{,y} \end{Bmatrix} + \begin{Bmatrix} w_{,x}w_{o,x} \\ w_{,y}w_{o,y} \\ w_{,x}w_{o,y} + w_{,y}w_{o,x} \end{Bmatrix} \tag{2.21a}$$

Or

$$\{\varepsilon\} = \{\varepsilon_o^p\} + z\{\varepsilon_o^b\} + \{\varepsilon_L^p\} + \{\varepsilon_I^p\} \tag{2.21b}$$

where

$\{\varepsilon_o^p\}$ is the linear strain due to inplane deformation.

$\{\varepsilon_o^b\}$ is the linear strain due to bending deformation.

$\{\varepsilon_L^p\}$ is the nonlinear strain due to inplane deformation.

$\{\varepsilon_I^p\}$ is the nonlinear strain due to initial deformation.

2.2.2 Stress-Strain Relations

Each orthotropic layer of the plate has known elastic constants. The stress-strain relation of any particular layer, with one of the axes of orthotropy coinciding with one of the principle axis, is given by

$$\begin{Bmatrix} \sigma_x \\ \sigma_y \\ \sigma_z \\ \tau_{xy} \\ \tau_{xz} \\ \tau_{yz} \end{Bmatrix} = \begin{bmatrix} C_{11} & C_{12} & C_{13} & C_{14} & 0 & 0 \\ C_{21} & C_{22} & C_{23} & C_{24} & 0 & 0 \\ C_{31} & C_{32} & C_{33} & C_{34} & 0 & 0 \\ C_{41} & C_{42} & C_{43} & C_{44} & 0 & 0 \\ 0 & 0 & 0 & 0 & C_{55} & C_{56} \\ 0 & 0 & 0 & 0 & C_{65} & C_{66} \end{bmatrix}_{sym.} \begin{Bmatrix} \varepsilon_x \\ \varepsilon_y \\ \varepsilon_z \\ \gamma_{xy} \\ \gamma_{xz} \\ \gamma_{yz} \end{Bmatrix} \tag{2.22}$$

Since normal stress σ_z is small, it can be neglected. The corresponding strain ε_z can be eliminated from Equations (2.22) by putting σ_z equal to zero. We also omit τ_{xz} and τ_{yz} from Equations (2.22) since we are not considering transverse shear effects in this study. This results in a reduced stress-strain relationship as

$$\begin{Bmatrix} \sigma_x \\ \sigma_y \\ \tau_{xy} \end{Bmatrix} = \begin{bmatrix} C_{11}^{'} & C_{12}^{'} & C_{13}^{'} \\ C_{21}^{'} & C_{22}^{'} & C_{23}^{'} \\ C_{31}^{'} & C_{32}^{'} & C_{33}^{'} \end{bmatrix} \begin{Bmatrix} \varepsilon_x \\ \varepsilon_y \\ \gamma_{xy} \end{Bmatrix} \tag{2.23}$$

where $C_{ij}^{'} = C_{ij} - C_{i3}C_{j3}/C_{33}$ for $i, j = 1,2,3$.

For a particular case where fibers are oriented at an angle θ with the *x*-axis, the transformed stress-strain relation for a laminae will be [79]

$$\begin{Bmatrix}\sigma_x\\ \sigma_y\\ \tau_{xy}\end{Bmatrix}=\begin{bmatrix}Q_{11} & Q_{12} & Q_{13}\\ Q_{12} & Q_{22} & Q_{23}\\ Q_{13} & Q_{23} & Q_{33}\end{bmatrix}\begin{Bmatrix}\varepsilon_x\\ \varepsilon_y\\ \gamma_{xy}\end{Bmatrix} \tag{2.24}$$

where

$$Q_{11} = C_{11}^{'}\cos^4\theta + 2(C_{12}^{'} + 2C_{33}^{'})\cos^2\theta\sin^2\theta + C_{22}^{'}\sin^4\theta$$

$$Q_{12} = (C_{11}^{'} + C_{22}^{'} - 4C_{33}^{'})\cos^2\theta\sin^2\theta + C_{12}^{'}(\cos^4\theta + \sin^4\theta)$$

$$Q_{22} = C_{11}^{'}\sin^4\theta + 2(C_{12}^{'} + 2C_{33}^{'})\cos^2\theta\sin^2\theta + C_{22}^{'}\cos^4\theta$$

$$Q_{33} = (C_{11}^{'} + C_{22}^{'} - 2C_{12}^{'} - 2C_{33}^{'})\cos^2\theta\sin^2\theta + C_{33}^{'}(\cos^4\theta + \sin^4\theta)$$

$$Q_{13} = (C_{11}^{'} - 2C_{33}^{'} - C_{12}^{'})\cos^3\theta\sin\theta + (C_{12}^{'} - C_{22}^{'} + 2C_{33}^{'})\cos\theta\sin^3\theta$$

$$Q_{23} = (C_{11}^{'} - 2C_{33}^{'} - C_{12}^{'})\cos\theta\sin^3\theta + (C_{12}^{'} - C_{22}^{'} + 2C_{33}^{'})\cos^3\theta\sin\theta$$

…… (2.25)

2.2.3 Stress Resultant-Strain Relation

Consider the linear strain terms in Equation (2.21). Combining these strain terms with the laminate constitutive equations given by Equations (2.24) and integrating layer-by-layer over the thickness, one obtains the following relations of stress resultants as

$$N_x, M_x = \int_{-t/2}^{t/2}\sigma_x(1, z)\,dz$$

$$N_y, M_y = \int_{-t/2}^{t/2} \sigma_y (1, z)\, dz \tag{2.26}$$

$$N_{xy}, M_{xy} = \int_{-t/2}^{t/2} \tau_{xy} (1, z)\, dz$$

The above equations can be cast in matrix form as

$$\begin{Bmatrix} N_x \\ N_y \\ N_{xy} \\ M_x \\ M_y \\ M_{xy} \end{Bmatrix} = \begin{bmatrix} A_{11} & A_{12} & A_{13} & B_{11} & B_{12} & B_{13} \\ & A_{22} & A_{23} & B_{21} & B_{22} & B_{23} \\ & & A_{33} & B_{31} & B_{32} & B_{33} \\ & & & D_{11} & D_{12} & D_{13} \\ & sym & & & D_{22} & D_{23} \\ & & & & & D_{33} \end{bmatrix} \begin{Bmatrix} \varepsilon_x^o \\ \varepsilon_y^o \\ \gamma_{xy}^o \\ \kappa_x \\ \kappa_y \\ \kappa_{xy} \end{Bmatrix} \tag{2.27}$$

where $\kappa_x, \kappa_y, \kappa_{xy}$ are the linear strains due to bending deformation.

Or in compact notation

$$\{N\} = [D]\{\varepsilon^o\} \tag{2.28}$$

Elements of membrane stiffness matrix [*A*], membrane-bending coupling matrix [*B*], bending stiffness matrix [*D*] are

$$(A_{ij}, B_{ij}, D_{ij}) = \int_{-t/2}^{t/2} Q_{ij} (1, z, z^2)\, dz \tag{2.29}$$

2.2.4 Finite Element Formulation

Based on the above theory, a finite element is developed using a bilinear isoparametric rectangular element. Each node of the element has six degrees of freedom given as

$$\{u, v, w, w_{,x}, w_{,y}, w_{,xy}\}$$

within the element, displacements can be interpolated in terms of the nodal degrees of freedom by adopting

a) Bilinear interpolation functions for the in-plane displacement *u* and *v* given by

$$u = \sum_i N_i u_i \quad \text{and} \quad v = \sum_i N_i v_i \qquad (i=1,..,4)$$

where *u* and *v* are the displacements in the *x* and *y*-directions, respectively, at any point in the element and u_i, v_i are their values at node *i* of that particular element. N_i is the interpolation function, which in the natural coordinate system shown in Figure (2.3) is

$$N_i = \frac{1}{4}(1 + rr_i)(1 + ss_i) \qquad (2.31)$$

where *i* is the function number and r_i = -1,1,1,-1; s_i=-1,-1,1,1 for *i*=1,..,4 respectively.

b) The transverse displacement *w* is interpolated using Hermite Cubic interpolation functions, which can be given in explicit form as

$$w(x,y)=\begin{bmatrix} f_1 & g_1 & h_1 & k_1 & \cdots & \cdots & f_4 & g_4 & h_4 & k_4 \end{bmatrix}\begin{Bmatrix} w_1 \\ w_{,x1} \\ w_{,y1} \\ w_{,xy1} \\ \vdots \\ \vdots \\ w_4 \\ w_{,x4} \\ w_{,y4} \\ w_{,xy4} \end{Bmatrix} \qquad (2.32a)$$

where for i=1,..,4 we have

$$f_i=\frac{1}{16}(r+r_i)^2(rr_i-2)(s+s_i)^2(ss_i-2)$$

$$g_i=-\frac{a}{32}r_i(r+r_i)^2(rr_i-1)(s+s_i)^2(ss_i-2) \qquad (2.32b)$$

$$h_i=-\frac{b}{32}(r+r_i)^2(rr_i-2)s_i(s+s_i)^2(ss_i-1)$$

$$k_i=\frac{ab}{64}r_i(r+r_i)^2(rr_i-1)s_i(s+s_i)^2(ss_i-1)$$

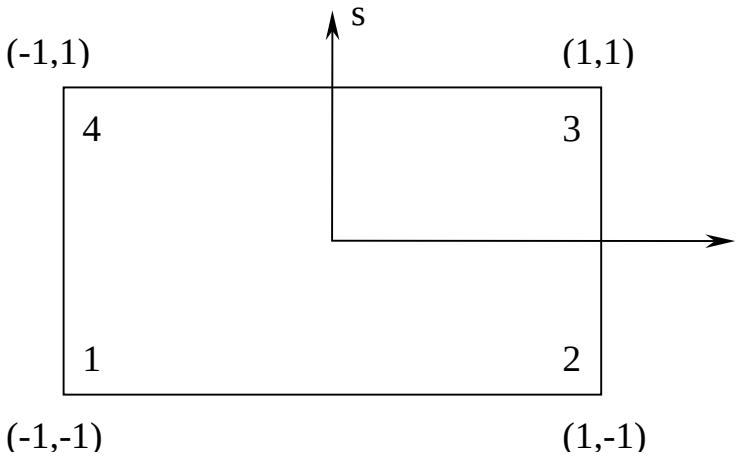

Figure (2.3) Element natural coordinate system and node numbering

Thus, we can express the displacement in terms of nodal degrees of freedom and using the previously defined shape functions. For instance,

$$\begin{Bmatrix} u \\ v \\ w \end{Bmatrix} = [N]\bar{a}^e \tag{2.33}$$

where $\bar{a}^e$ is the element nodal displacement vector and [N] is the matrix of shape functions. For convenience the element nodal displacement vector $\bar{a}^e$ will be divided into those which influence in-plane and bending deformation respectively.

$$\bar{a}_i^e = \begin{Bmatrix} \bar{a}_i^p \\ \bar{a}_i^b \end{Bmatrix} \quad \text{with} \quad \bar{a}_i^p = \begin{Bmatrix} u_i \\ v_i \end{Bmatrix} \quad \text{and} \quad \bar{a}_i^b = \begin{Bmatrix} w_i \\ \dfrac{\partial w}{\partial x_i} \\ \dfrac{\partial w}{\partial y_i} \\ \dfrac{\partial^2 w}{\partial x_i \partial y_i} \end{Bmatrix} \tag{2.34}$$

Thus the shape functions can also be subdivided as

$$[N_i] = \begin{bmatrix} N_i^p & 0 \\ 0 & N_i^b \end{bmatrix} \tag{2.35}$$

2.2.5 Evaluation of the Linear Stiffness Matrix $[K_o]$

Substituting Equations (2.31) and (2.32) into the linear strain components of Equation (2.21) we get

$$\begin{Bmatrix} \varepsilon_x^o \\ \varepsilon_y^o \\ \gamma_{xy}^o \\ \kappa_x \\ \kappa_y \\ \kappa_{xy} \end{Bmatrix} = \begin{bmatrix} N_{1,x} & 0 & N_{2,x} & 0 & N_{3,x} & 0 & N_{4,x} & 0 & & & & & & & & \\ 0 & N_{1,y} & 0 & N_{2,y} & 0 & N_{3,y} & 0 & N_{4,y} & & & & 0 & & & & \\ N_{1,y} & N_{1,x} & N_{2,y} & N_{2,x} & N_{3,y} & N_{3,x} & N_{4,y} & N_{4,x} & & & & & & & & \\ & & & & & & & & -f_{1,xx} & -g_{1,xx} & -h_{1,xx} & -k_{1,xx} & \cdots & \cdots & -k_{4,xx} \\ & & & 0 & & & & & -f_{1,yy} & -g_{1,yy} & -h_{1,yy} & -k_{1,yy} & \cdots & \cdots & -k_{4,yy} \\ & & & & & & & & 2f_{1,xy} & 2g_{1,xy} & 2h_{1,xy} & 2k_{1,xy} & \cdots & \cdots & 2k_{4,xy} \end{bmatrix} \begin{Bmatrix} u_1 \\ v_1 \\ \vdots \\ v_4 \\ w_1 \\ w_{,x1} \\ w_{,y1} \\ w_{,xy1} \\ \vdots \\ \vdots \\ w_{,y4} \\ w_{,xy4} \end{Bmatrix}$$

… … (2.36a)

In a short form

$$\{\varepsilon^o\} = [B_o]\{\bar{a}^e\} \tag{2.36b}$$

Internal strain energy (due to linear strain only) can now be determined by integrating the products of strains and stress resultants over the area of an element, i.e.

$$\pi = \frac{1}{2}\int_A \{\varepsilon\}^T \{N\}\, dA \tag{2.37}$$

where $\{\varepsilon\}$ includes all linear strains and $\{N\}$ is the vector of stress resultants defined in Equations (2.27). Substituting Equations (2.28) and (2.36) for $\{\varepsilon\}$ and $\{N\}$ into (2.37) we get

$$\pi = \frac{1}{2}\int_A \{\bar{a}^e\}[B_o]^T [D][B_o]\{\bar{a}^e\} dA \tag{2.38}$$

In a concise form

$$\pi = \frac{1}{2}\{\bar{a}^e\}^T [K_o]\{\bar{a}^e\} \tag{2.39}$$

where

$$[K_o] = \int_A [B_o]^T [D][B_o]\, dA \tag{2.40}$$

is the linear stiffness matrix for the element.

2.2.6 Evaluation of the Initial Displacement Matrix $[K_L]$

In order to be able to evaluate the element large displacement stiffness matrix $[K_L]$, it will be necessary to establish an expression for $[\overline{B}]$. First we shall note that

$$[\overline{B}] = [B_o] + [B_L] \tag{2.41}$$

where $[B_o] = \begin{bmatrix} B_o^p & 0 \\ 0 & B_o^b \end{bmatrix}$ and $[B_L] = \begin{bmatrix} 0 & B_L^b \\ 0 & 0 \end{bmatrix}$

where $[B_o]$ is defined in Equation (2.36) and $[B_L^b]$ is found by taking the variation of the nonlinear strain components $\{\varepsilon_L^p\}$ with respect to the parameters $\{\bar{a}^b\}$. This nonlinear strain component of Equation (2.21) can be written in a more convenient form as

$$\{\varepsilon_L^p\}=\begin{Bmatrix}\frac{1}{2}(\frac{\partial w}{\partial x})^2\\ \frac{1}{2}(\frac{\partial w}{\partial y})^2\\ (\frac{\partial w}{\partial x})(\frac{\partial w}{\partial y})\end{Bmatrix}=\frac{1}{2}\begin{bmatrix}\frac{\partial w}{\partial x} & 0\\ 0 & \frac{\partial w}{\partial y}\\ \frac{\partial w}{\partial y} & \frac{\partial w}{\partial x}\end{bmatrix}\begin{Bmatrix}\frac{\partial w}{\partial x}\\ \frac{\partial w}{\partial y}\end{Bmatrix}=\frac{1}{2}[A]\{\theta\} \tag{2.42}$$

The derivatives (slopes) of *w* can be related to the nodal parameters $\{\bar{a}^b\}$ as

$$\{\theta\}=\begin{Bmatrix}\frac{\partial w}{\partial x}\\ \frac{\partial w}{\partial y}\end{Bmatrix}=[G]\{\bar{a}^b\} \tag{2.43}$$

in which we have

$$[G]=\begin{bmatrix}f_{1,x} & g_{1,x} & h_{1,x} & k_{1,x} & \cdots & \cdots & k_{4,x}\\ f_{1,y} & g_{1,y} & h_{1,y} & k_{1,y} & \cdots & \cdots & k_{4,y}\end{bmatrix} \tag{2.44}$$

Taking the variation of Equation (2.42) we have [80]

$$d\{\varepsilon_L^p\}=\frac{1}{2}d[A]\{\theta\}+\frac{1}{2}[A]d\{\theta\}=[A]d\{\theta\}=[A][G]d\{\bar{a}^b\} \tag{2.45}$$

and hence immediately, by definition

$$[B_L^b]=[A][G] \tag{2.46}$$

In order incorporate the imperfections in the formulation we consider now the strain due to imperfections as given by Equation (2.21)

$$\{\varepsilon_I^p\} = \begin{Bmatrix} w_{,x} w_{o,x} \\ w_{,y} w_{o,y} \\ w_{,x} w_{o,y} + w_{,y} w_{o,x} \end{Bmatrix} \tag{2.47}$$

Once again, the imperfection strain components can be written as

$$\{\varepsilon_I^p\} = \frac{1}{2} \begin{bmatrix} 2w_{o,x} & 0 \\ 0 & 2w_{o,y} \\ 2w_{o,y} & 2w_{o,x} \end{bmatrix} \begin{Bmatrix} \frac{\partial w}{\partial x} \\ \frac{\partial w}{\partial y} \end{Bmatrix} = \frac{1}{2} [A_2] \{\theta\} \tag{2.48}$$

Following the same analysis as for the nonlinear strains, we can finally combine the effect of the two strains into one $[B_L^b]$ defined as

$$[B_L^b] = [A_3][G] \tag{2.49}$$

where

$$[A_3] = \begin{bmatrix} w_{,x} + 2w_{o,x} & 0 \\ 0 & w_{,y} + 2w_{o,y} \\ w_{,y} + 2w_{o,y} & w_{,x} + 2w_{o,x} \end{bmatrix}$$

In this study, the imperfection function is assumed to vary bilinearly over the element area

$$w_o(r,s) = c_1 + c_2\, r + c_3\, s + c_4\, rs \tag{2.50}$$

where c_1, c_2, c_3 and c_4 are unknown constants that are directly related to the nodal values of imperfection for the specific element. Notice that values of the nodal imperfections are obtained from the series representation of the imperfect profile that will be described in Chapter 4 of this study.

The nonlinear stiffness matrix $[K_L]$ as defined in Equation (2.16) can now be calculated as

$$[K_L] = \int_A [B_o]^T [D][B_L] + [B_L]^T [D][B_L] + [B_L]^T [D][B_o] dA$$

2.2.7 Evaluation of the Initial Stress Stiffness Matrix $[K_\sigma]$

Finally the initial stress stiffness matrix has to be found using the definition of Equation (2.17). By taking the variation of Equation (2.41) we have

$$d[B_L]^T = \begin{bmatrix} 0 & 0 \\ d[B_L^b]^T & 0 \end{bmatrix} \tag{2.51}$$

which on substitution into Equations (2.17) and (2.49) gives

$$[K_\sigma] d\bar{a} = \int_A \begin{bmatrix} 0 & 0 \\ [G]^T d[A]^T & 0 \end{bmatrix} \begin{Bmatrix} N_x \\ N_y \\ N_{xy} \\ M_x \\ M_y \\ M_{xy} \end{Bmatrix} dA \tag{2.52}$$

However, using the mathematical properties of the matrix [*A*], we can write [80]

$$d[A]^T \begin{Bmatrix} N_x \\ N_y \\ N_{xy} \end{Bmatrix} = \begin{bmatrix} N_x & N_{xy} \\ N_{xy} & N_y \end{bmatrix} [G] d\bar{a}^b$$

and finally we obtain

$$[K_\sigma] = \begin{bmatrix} 0 & 0 \\ 0 & [K_\sigma^b] \end{bmatrix} \tag{2.53}$$

with

$$[K_\sigma^b] = \int_A [G]^T \begin{bmatrix} N_x & N_{xy} \\ N_{xy} & N_y \end{bmatrix} [G]\, dA \tag{2.54}$$

Recall that the stress resultants are defined in terms of the element strains and thus in terms of the element displacements and shape functions through Equations (2.27) and (2.21).

2.2.8 Applied Load Vector

A consistent load vector is developed for the out-of-plane loading using the principle of virtual work

$$\{F_i\} = \int_A q(x,y) \begin{Bmatrix} 0 \\ 0 \\ f_i \\ g_i \\ h_i \\ k_i \end{Bmatrix} dA \qquad i = 1,\ldots,4 \tag{2.55}$$

where $q(x,y)$ is the out of plane load distribution. The inplane loading is applied directly at the nodes as concentrated forces in the x and y-directions. Combining the nodal load vectors $\{F_i\}$, the element vector $\{F_e\}$ can be obtained as

$$\{F_e\} = [F_1 \quad F_2 \quad F_3 \quad F_4]^T$$

2.3 Hybrid Numerical-Analytical Integration

In order to perform the finite element analysis, the matrices defining element properties, e.g. stiffness matrices, have to be computed. In a previous study by the author [81], it was concluded that the use of analytical closed form integration (using symbolic manipulation computer programs) in the evaluation of the element matrices in the linear analysis case leads to a reduced computation time in addition to an increase in the accuracy of the obtained results compared to the usual Gauss Quadrature integration schemes [80]. However, in the present nonlinear analysis, the tangent stiffness matrix is function of the element nodal degrees of freedom, which makes the use of analytical integration out of reach due to the increased size of the expressions to be integrated. A new hybrid integration technique that mixes both Gauss Quadrature and symbolic manipulation together was introduced in this study.

To better describe the new technique, let's consider the case of the linear stiffness matrix given by

$$[K_o] = \frac{ab}{4} \int_{-1}^{1} \int_{-1}^{1} [B_o]^T [D][B_o] \, dr ds$$

First, we start by evaluating the integrand in a closed form

$$[\hat{K}] = [B_o]^T [D][B_o] \tag{2.56}$$

Notice that, terms of the matrix $[\hat{K}]$ are functions of (r, s), element dimensions (a, b) and element constitutive coefficients D_{ij}.

In the second phase of the process, the matrix $[K_o]$ is obtained by numerically integrating $[\hat{K}]$ as follows:

$$K_o(i,j) = \frac{ab}{4}\sum_{j=1}^{4}\sum_{i=1}^{4} H_i * H_j * \hat{K}(i,j)\Big|_{(r_i,s_j)} \tag{2.57}$$

Table (2.1) shows the values of the Gaussian points (r_i, s_i) and the corresponding weighting coefficients H_i. Applying Equation (2.58) leads to closed form expressions for the terms of the stiffness matrix $[K_o]$ as functions of the element dimensions and constitutive coefficients.

Table (2.1) Abscissae and weight coefficients of the Gaussian quadrature formula

$\pm r_i$	H_i
0.86113 63115 94053	0.34785 48451 37454
0.33998 10435 84856	0.65214 51548 62546

2.4 The Frontal Equation Solution Technique

At any load step (i) during the incremental solution of the nonlinear problem, it is required to solve a system of linear equations in the nodal degrees of freedom in the form

$$[K_T^{i-1}]\Delta\vec{u}^{\,i} = \Delta\vec{f}^{\,i} \tag{2.58}$$

where $[K_T^{i-1}]$ is the tangent stiffness matrix evaluated at the previous load step, $\Delta\vec{f}^{\,i}$ is the load increment and $\Delta\vec{u}^{\,i}$ is the resulting displacement increment. The method adopted to solve this system of equations is a major factor influencing the efficiency of the finite

element program. Several options are open to the programmer ranging from iterative methods such as the Gauss-Seidel technique [82] to the direct Gaussian elimination algorithms. In this study we shall employ a direct elimination process and in particular the frontal method of equation assembly and reduction. The frontal equation solution technique was originated by Irons [83] and has earned the reputation of being easy and inexpensive.

The frontal method can be considered as a particular technique for first assembling finite elements stiffnesses and nodal forces into a global stiffness matrix and load vector and then solving for the unknown displacement by means of a Gaussian elimination and back substitution process. It is designed to minimize core storage requirements, and the number of arithmetic operations.

No attempt will be made here to give a full detailed description of the frontal technique. Such detailed presentation can be found in [84]. The frontal technique as described in this study is applicable only to the solution of symmetric systems of linear stiffness equations. Since the tangent stiffness matrix has been derived previously from a variational principle, it is thus symmetric by definition [80]. Furthermore, even though the problem is nonlinear by nature, we are using an incremental approach where the system is transformed into a series of linearized systems of equations at each load increment. This enables us to use the frontal technique at each load step.

The main idea of the frontal solver solution is to assemble the equations and eliminate the variables at the same time. As soon as the coefficients of an equation are completely assembled from the contributions of all relevant elements, the corresponding variable can be eliminated. Therefore, the complete structural stiffness matrix is never formed as such, since after elimination the reduced equation is immediately transferred to back-up disc storage.

The core contains, at any given instant, the upper triangular part of a square matrix containing the equations which are being formed at that particular time. These

equations, their corresponding nodes and degrees of freedom are termed the *front*. The number of unknowns in the front is the *frontwidth*; this length generally changes continually during the assembly/reduction process. The maximum size of the problem that can be solved is governed by the maximum frontwidth. The equations, nodes and degrees of freedom belonging to the front are termed *active*; those which are yet to be considered are *inactive*; those which have passed through the front and have been eliminated are said to be *deactivated*.

During the assembly/elimination process the elements are considered each in turn according to a prescribed order. Whenever a new element is called in, its stiffness coefficients are read from a file and summed either into existing equations, if the nodes are already active, or into new equations which have to be included in the front if the nodes are being activated for the first time. If some nodes are appearing for the last time, the corresponding equations can be eliminated and stored away in a file and are thus deactivated. In so doing they free space in the front which can be employed during assembly of the next element. More details concerning the technique are presented by Hinton [84].

2.5 Incremental Procedure for Solution of Nonlinear Discrete Problems

The discretized nonlinear system of equations can be written as a set of algebraic equations in the form

$$[K_T(\bar{a})]\bar{a} - \bar{f} = 0 \tag{2.59}$$

where $\bar{f}$ is the external force and $\bar{a}$ is the structural displacement. Both are generally zero at the start of the problem. The incremental procedure makes use of the fact that the solution for $\bar{a}$ is known when the load term $\bar{f}$ is zero. In such circumstances, it is convenient to study the behavior of $\bar{a}$ as the vector $\bar{f}$ is incremented.

Such a method can yield reasonable results and guaranteed to converge if a suitably small increment of $\vec{f}$ is chosen. Furthermore, the intermediate results provide useful information on the loading process.

To explain the method it is convenient to rewrite Equation (2.59) as

$$[K_T(\bar{a})]\bar{a} - \lambda\, \vec{f}_o = 0 \tag{2.60}$$

where $$\vec{f} = \lambda\, \vec{f}_o$$

On differentiation of Equation (2.60) with respect to λ, this results in

$$[K_T(\bar{a})]\frac{d\bar{a}}{d\lambda} - \vec{f}_o = 0 \tag{2.61a}$$

or

$$\frac{d\bar{a}}{d\lambda} = [K_T(\bar{a})]^{-1}\, \vec{f}_o \tag{2.61b}$$

where $[K_T]$ is the tangential stiffness matrix previously described.

The problem posed in Equation (2.61b) is a classical one of numerical analysis for which many solution (integration) techniques are available. The simplest one (Euler method) states

$$\bar{a}^{i+1} - \bar{a}^{i} = [K_T(\bar{a}^{i})]^{-1}\, \vec{f}_o\, \Delta\lambda^{i} = [K_T^{i}]^{-1}\, \Delta\vec{f}^{\,i} \tag{2.62}$$

where the superscript refers to the increments of λ or $\vec{f}$, i.e.,

$$\lambda^{i+1} = \lambda^{i} + \Delta\lambda$$

or (2.63)

$$\vec{f}^{\,i+1} = \vec{f}^{\,i} + \Delta\vec{f}$$

Figure (2.4) illustrates this incremental process.

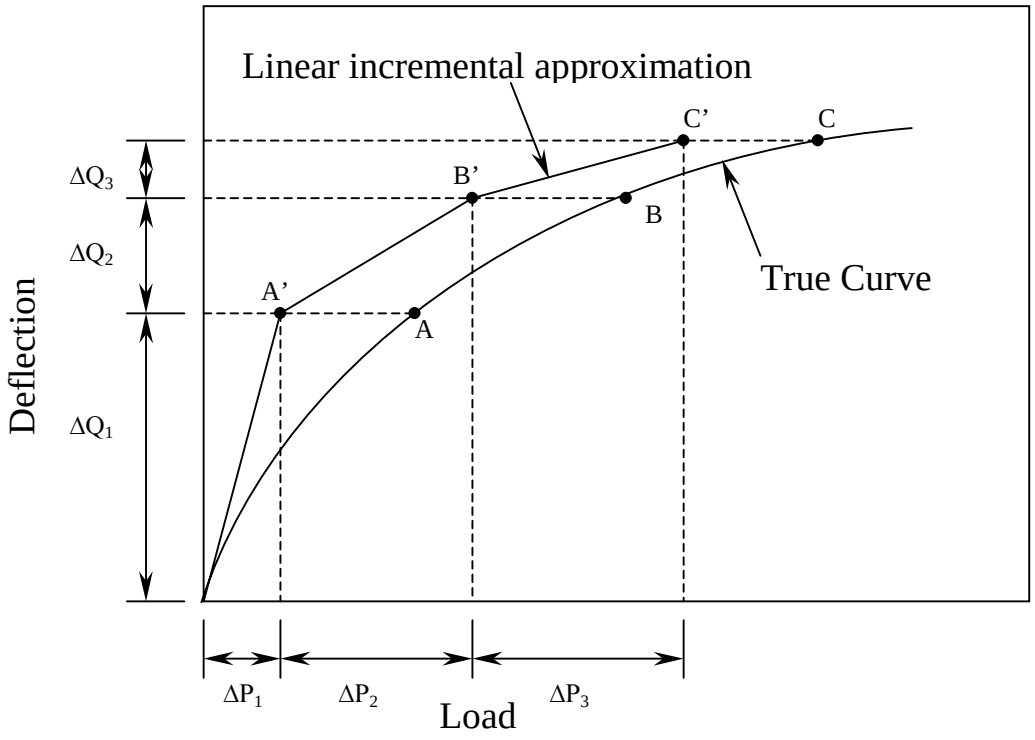

Figure (2.4) Load-deflection curve by piecewise linear incremental approach

Note that improved integration schemes, such as the various predictor-corrector of Runge-Kutte formulae, improve accuracy but with an additional increase in cost. Thus these schemes will not be employed in this study.

2.6 Numerical Examples

2.6.1 Large Deflection of an Uniformly Loaded Square Plate without Imperfections

Analysis is carried out in a case of an isotropic plate with clamped edges ($1\,m \times 1m \times 2\,mm, E = 2\times10^4\,kg/mm^2, \nu = 0.3$) and a distributed load acting upward. Because of the symmetry of the plate, a quarter of the plate is sufficient to be analyzed, as shown in Figure (2.5). The boundary conditions are given as follows

on *OA*	$w_{,y} = 0\,,\ v = 0$
on *AB* and *BC*	$w = w_{,x} = w_{,y} = 0\,,\ u = v = 0$
on *CO*	$w_{,x} = 0\,,\ u = 0$

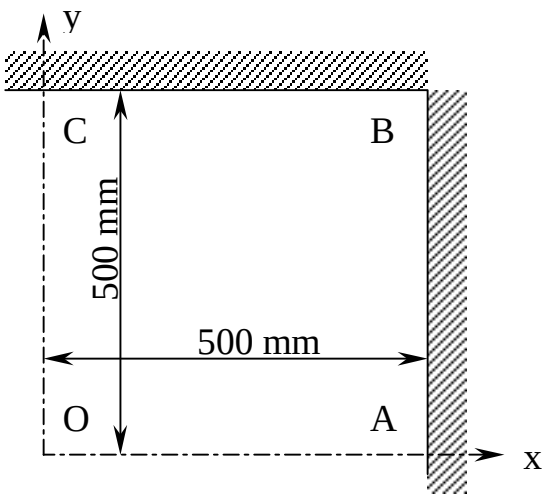

Figure (2.5) Square plate with all edges clamped (a quarter of total region)

The region to be analyzed, *OABC,* is divided into 25 elements (36 nodes) as shown in Figure (2.6). The out-of-plane displacement of point *O* is plotted in Figure (2.7) as the load intensity is increased. Results are compared with the analytical solution

obtained by S. Way [85]. A good agreement is observed. In Figure (2.8), upper and lower fiber stresses at node *O* are shown and compared to the Finite Element nonlinear solutions obtained by Kawai [88]. Finally the load intensity is fixed at $0.8\times10^{-4}\,kg/mm^2$ and the number of load increments used in the analyses is varied. Figure (2.9) shows the convergence of the out of plane deflection at point *O* as the number of load increments increases.

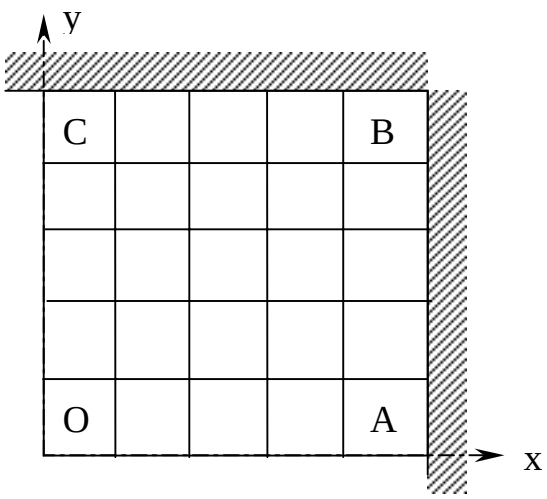

Figure (2.6) Finite element mesh employed

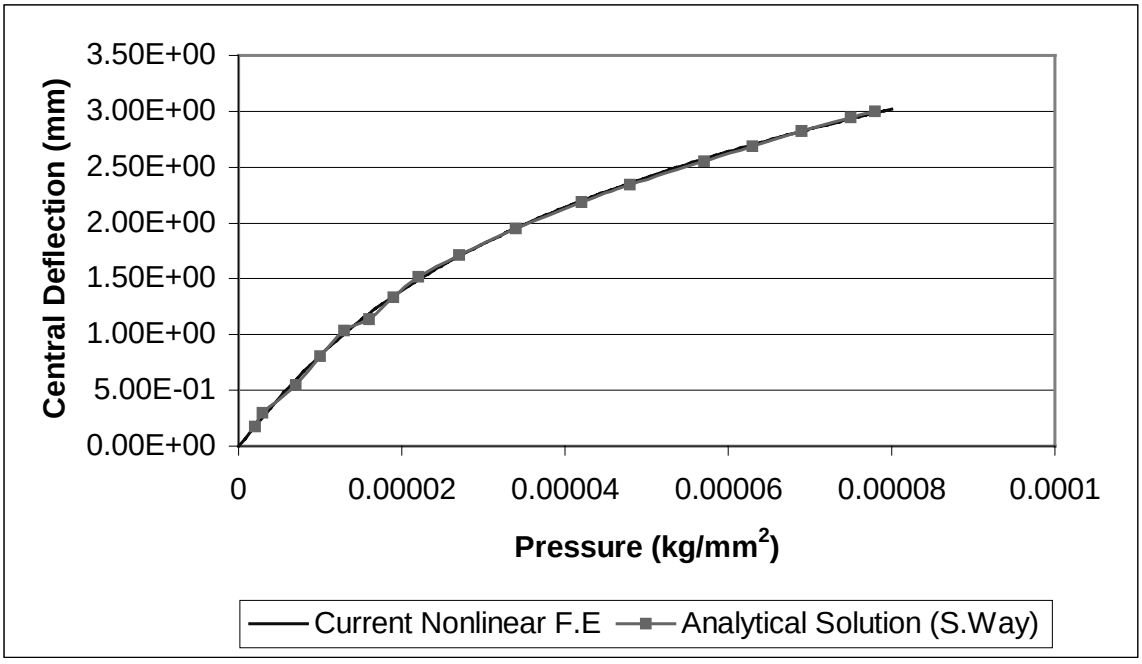

Figure (2.7) Load-deflection curve at point *O* of a square plate with all edges clamped under uniform load

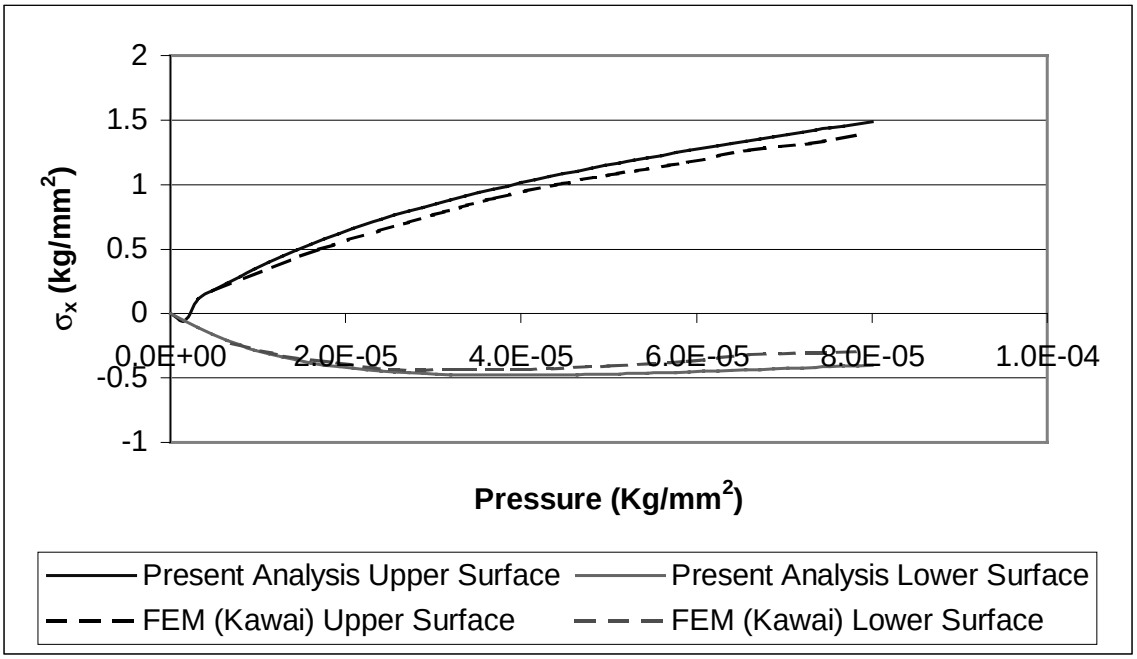

Figure (2.8) Upper and lower stress at point *O* of the square plate

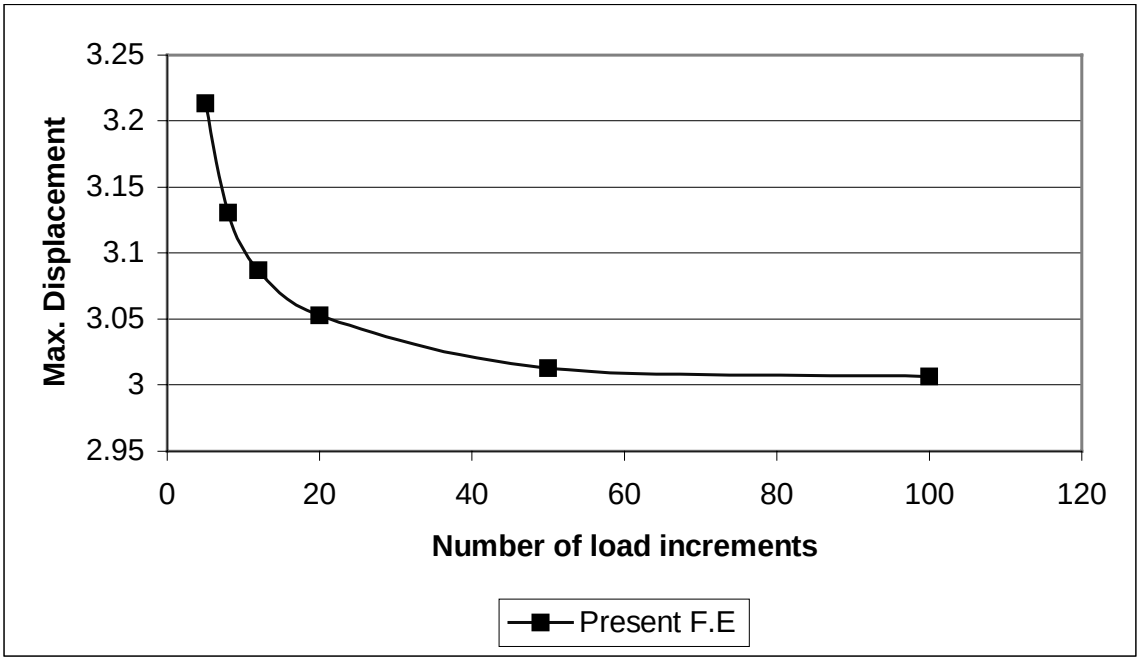

Figure (2.9) Maximum deflection convergence as the number of load increments increases

2.6.2 Large Deflection of a Uniformly Loaded CCCC Square Plate with Initial Imperfection

In this section we consider the central deflections of square plates with all edges clamped and with initial deflection. The initial deflection is assumed as to satisfy the boundary conditions and is given by

$$w_o(x,y) = W_o \sin^2(\frac{\pi x}{L}) \sin^2(\frac{\pi y}{L}) \tag{2.64}$$

where L is the side length of the plate. Four cases where W_o is equal to 0, 0.5h, and 2h, where h is the plate thickness, are considered. The same plate dimensions and material properties used in the previous section are employed here. The same 25-element grid over one-quarter of the plate is used. The results for pressure vs. center deflection are shown in

Figure (2.10). The alternative analytic solutions for the plate with no initial deflection are available in [86]. In this reference, Levy replaced the edge bending moment by equivalent pressure distribution and then applied the general Fourier series solution for the simply supported plate. Levy's results for center deflection are also shown in Figure (2.10). Very good agreement is observed.

2.6.3 Large Deflection of a Square Plate under a Concentrated Load with Two Opposite Edges Clamped and the Other Two Free

In this section we consider a square plate with no imperfection under a concentrated load P_N applied at point N as shown in Figure (2.11). Considering the symmetry of the problem, only the upper half of the plate is analyzed. The region under consideration is divided into 50 elements.

In Figure (2.12) the displacements of nodes A and B are plotted with the experimental values given by Kawai [88]. Again good agreement is observed between Finite Element and experimental results.

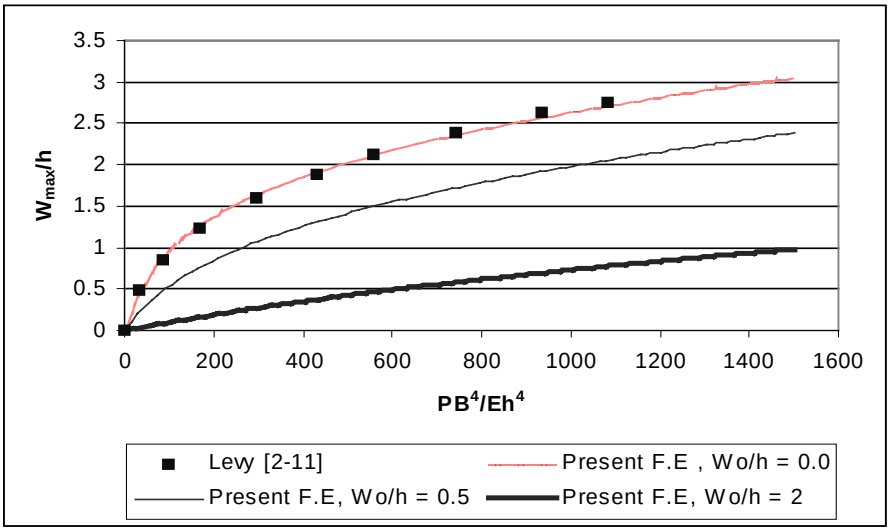

Figure (2.10) Center deflection of CCCC square plates with imperfections

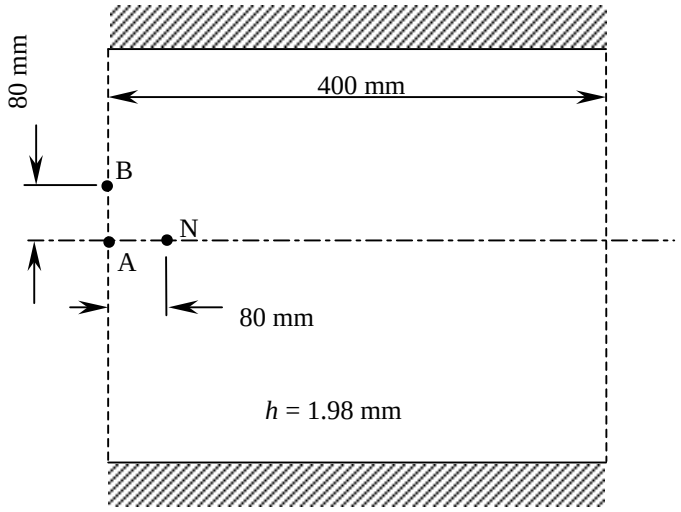

Figure (2.11) Square plate with two edges clamped and the other two free
($E = 2.15\times10^4\ kg/mm^2, \nu = 0.3$ **)**

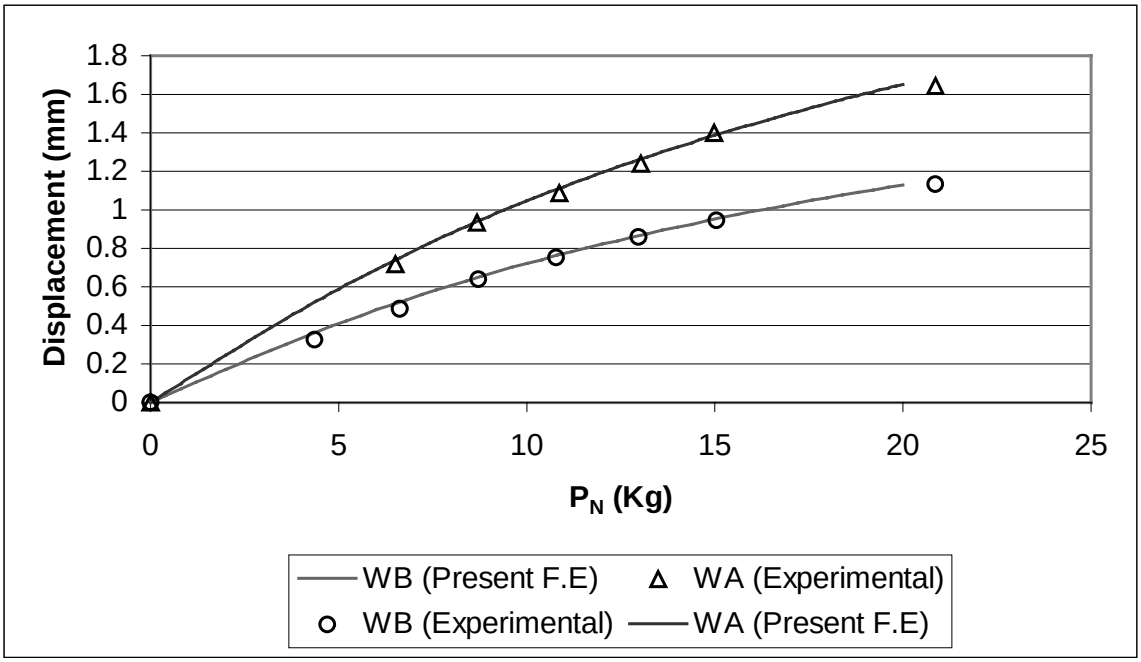

Figure (2.12) Load-deflection curves at points A and B of a square plate under concentrated load

2.6.4 Postbuckling Response and Failure Prediction of Graphite-Epoxy Plates Loaded in Compression

The postbuckling and failure characteristics of flat, rectangular graphite-epoxy panels with and without holes that are loaded in axial compression have been examined in an experimental study by Starnes and Rouse [89]. The panels were fabricated from commercially available unidirectional Thornel 300 graphite-fiber tapes preimpregnated with 450 K cure Narmco 5208 thermosetting epoxy resin. Typical lamina properties for this graphite-epoxy system are 131.0 GPa for the longitudinal Young's modulus, 13.0 GPa for the transverse Young's modulus, 6.4 GPa for the inplane shear modulus, 0.38 for the major Poisson's ratio (ν_{12}), and 0.14 mm for the lamina thickness. Each panel was loaded in axial compression using a 1.33-MN capacity hydraulic testing machine. The loaded ends of the panel were clamped by fixtures during testing, and the unloaded edges were simply supported by knife-edge restrains to prevent the panels from buckling as wide columns. For more details about the test setup, or the experimental procedure, the reader is referred to the paper by Starnes and Rouse [89].

In this study only one panel from Ref. [89] is analyzed, and the analytical results are compared with the experimental results presented in Ref. [89]. The panel is 50.8 cm long x 17.8 cm wide, 24-ply orthotropic laminate with a $[\pm 45/0_2 \ \pm 45/0_2 \ \pm 45/0/90]_s$ stacking sequence. It is denoted as panel C4 in Ref. [89]. Panel C4 was observed in the test to buckle into two longitudinal half-waves and one transverse half-wave.

A finite element model for this panel was obtained using the element developed in this study. The modeling approach was based on using six finite elements per buckle half wave in each direction as recommended by Engelstad and Reddy [90]. Thus, six elements were used along the width of the panel, while twelve elements were needed along the length. The finite element mesh used is shown in Figure (2.13).

In order to efficiently proceed beyond the critical buckling point in the postbuckling analysis of the panel, an initial geometric imperfection in the same shape as the first buckling mode was assumed. The amplitude of each mode was selected to be 1-5% of the total laminate thickness. This means that an eccentricity is added to the initial geometry that allows efficient progress past the critical point, but does not affect the results in the postbuckling range.

Finally, the *maximum strain criterion* was used in this example to predict failure of this panel. Failure occurs if any one of the following conditions are satisfied

$$\varepsilon_{1c_c} > \varepsilon_1 \quad or \quad \varepsilon_1 > \varepsilon_{1c_t}$$

$$\varepsilon_{2c_c} > \varepsilon_2 \quad or \quad \varepsilon_2 > \varepsilon_{2c_t} \tag{2.65}$$

$$\gamma_{12} > \gamma_{12c}$$

where $\varepsilon_1, \varepsilon_2$ are the normal strains along the fiber and normal to the fiber, respectively, and γ_{12} is the in-plane shear strain. And $\varepsilon_{1c}, \varepsilon_{2c}$ correspond to the critical strains in the 1 and 2-directions, and the subscripts *t* and *c* denote tension and compression, respectively.

Comparisons between test results from [89] and finite element results from the present study are shown in Figures (2.14) and (2.15). End shortening *u* normalized by the analytical end shortening u_{cr} at buckling is shown as a function of the applied load *P* normalized by the analytical buckling load P_{cr}. The circles in this figure represent test data, and the curve represent analytical data determined from the nonlinear finite element analysis. A good correlation is observed between the experimental and the finite element results. Figure (2.15) shows the out-of-plane deflection *w* near a point of maximum deflection (node 32) normalized by the panel thickness *t* as a function of the normalized load. Results obtained from a commercial finite element package (ABAQUS) are also shown on the same figure. Notice that, in the ABAQUS analysis a curved shell element

was employed in contrast to the flat shell element developed in this study, however the total number of degrees of freedom was kept constant. From this graph we notice that the postbuckling response of this panel exhibits large out-of-plane deflections (nearly three time the panel thickness). This panel was analyzed by Reddy et al [91] using three different finite element formulations, one of which utilized the classical laminated plate theory with the effects of transverse shear neglected. In that work it was concluded that the presence of shear flexibility improved the element convergence characteristics, particularly when operating deep in the postbuckling regime. However, since we are more concerned in this study with the cost of the analysis (this analysis is to be used for optimization purposes), shear deformation will not be included in the formulation in order to avoid the large increase in computation time associated with such an extension.

In this chapter we presented a 4 node, 24 degree of freedom rectangular element for the geometrically nonlinear analysis of composite structures. A new integration technique that mixes symbolic closed form function manipulation and Gaussian quadrature numerical integration has been introduced in this study in order to reduce the required computation time for each analysis. Several example problems were presented, and finite element results were compared to analytical, experimental and other finite element results. A very good agreement was demonstrated for problems involving different sets of boundary conditions, loading and initial imperfection profiles. In the next chapter FEPA is linked to a genetic algorithm in order to obtain a design tool (FEPAD).

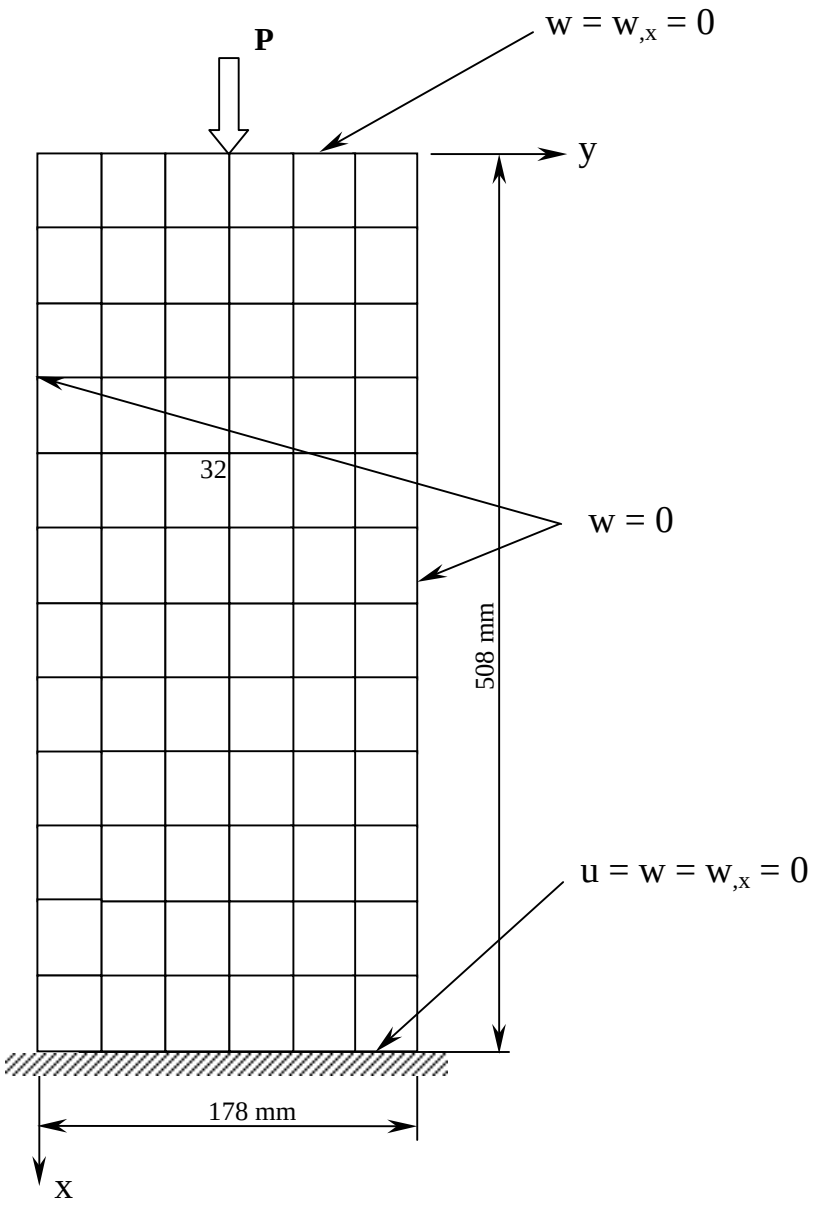

Figure (2.13) Finite Element Mesh and Boundary Conditions

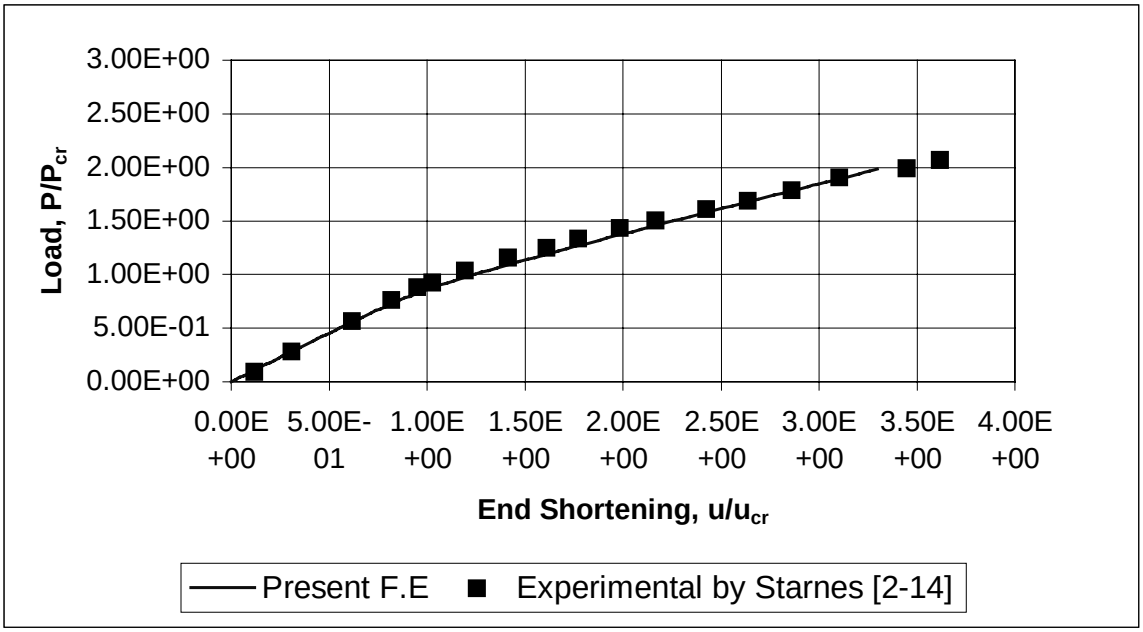

Figure (2.14) Postbuckling response characteristics : End Shortening

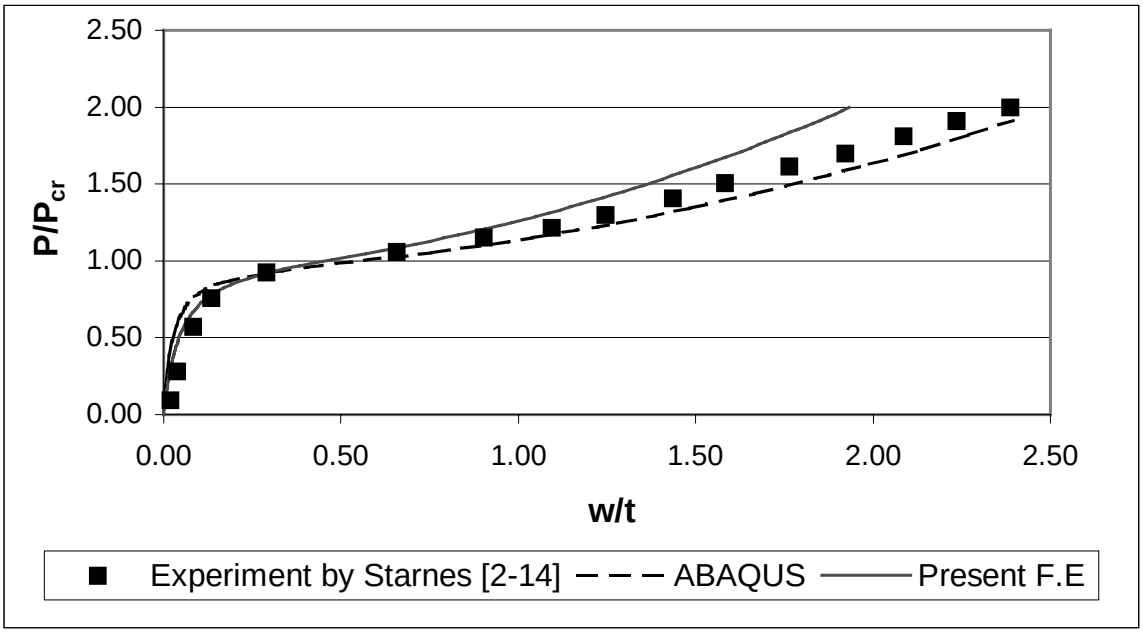

Figure (2.15) Postbuckling response characteristics : Out-of-plane deflection